Organic Electronics 13 (2012) 273–282

Contents lists available at SciVerse ScienceDirect

Organic Electronics

journal homepage: www.elsevier.com/locate/orgel

Synthesis and characterization of triphenylamine flanked thiazole-based small molecules for high performance solution processed organic solar cells

Pranabesh Dutta, Wooseung Yang, Seung Hun Eom, Soo-Hyoung Lee *

School of Semiconductor and Chemical Engineering, Chonbuk National University, Duckjin-dong 664-14, Jeonju 561 756, Republic of Korea

ARTICLE INFO

Article history:
Received 23 September 2011
Received in revised form 11 November 2011
Accepted 19 November 2011
Available online 9 December 2011

Keywords:
Donor–acceptor
Conjugated small molecules
Suzuki coupling
Thiazole derivatives
Organic solar cells
Power conversion efficiency

ABSTRACT

Two new small molecules, 5,5-bis(2-triphenylamino-3-decylthiophen-2-yl)-2,2-bithiazole (**M1**) and 2,5-bis(2-triphenylamino-3-decylthiophen-2-yl)thiazolo[5,4-d]thiazole (**M2**) based on an electron-donor triphenylamine unit and electron-acceptor thiophene–thiazolothiazole or thiophene–bithiazole units were synthesized by a palladium(0)-catalyzed Suzuki coupling reaction and examined as donor materials for application in organic solar cells. The small molecules had an absorption band in the range of 300–560 nm, with an optical band gap of 2.22 and 2.25 for **M1** and **M2**, respectively. As determined by cyclic voltammetry, the highest occupied molecular orbital and lowest unoccupied molecular orbital energy levels of **M1** were −5.27 eV and −3.05 eV, respectively, which were 0.05 eV and 0.02 eV greater than that of **M2**. Photovoltaic properties of the small molecules were investigated by constructing bulk-heterojunction organic solar cell (OSC) devices using **M1** and **M2** as donors and fullerene derivatives, 6,6-phenyl-C61-butyric acid methyl ester ($PC_{61}BM$) and 6,6-phenyl-C71-butyric acid methyl ester ($PC_{71}BM$) as acceptors with the device architecture ITO/PEDOT:PSS/**M1** or **M2**:PCBM/LiF/Al. The effect of the small molecule/fullerene weight ratio, active layer thickness, and processing solvent were carefully investigated to improve the performance of the OSCs. Under AM 1.5 G 100 mW/cm^2 illumination, the optimized OSC device with **M1** and $PC_{71}BM$ at a weight ratio of 1:3 delivered a power conversion efficiency (PCE) of 1.30%, with a short circuit current of 4.63 mA/cm^2, an open circuit voltage of 0.97 V, and a fill factor of 0.29. In contrast, **M2** produced a better performance under identical device conditions. A PCE as high as 2.39% was recorded, with a short circuit current of 6.49 mA/cm^2, an open circuit voltage of 0.94 V, and a fill factor of 0.39.

1. Introduction

The last few years have given rise to a remarkable development in bulk heterojunction polymer solar cells (PSC) after the introduction of low band gap (LBG) alternating donor–acceptor (D–A) conjugated polymers blended with fullerene derivatives such as 6,6-phenyl-C61-butyric acid methyl ester ($PC_{61}BM$) or 6,6-phenyl-C71-butyric acid methyl ester ($PC_{71}BM$) as photoactive donor materials [1]. Following the extensive efforts in the development of new LBG donor–acceptor conjugated polymers and device optimization, it is now possible to achieve PSC power conversion efficiency (PCE) above 7% [2]. Very recently, an outstanding PCE of 8.37% has further been accomplished with simultaneous enhancement in short circuit current (J_{sc}), open circuit voltage (V_{oc}), and fill factor (FF) by incorporation of a conjugated polyelectrolyte cathode interlayer in the solar cell device [2f], which additionally takes polymer solar cell research one step ahead towards realization for practical application and commercialization.

Solution-processable low molecular weight (LMW) organic semiconductors are potentially useful in exploiting

* Corresponding author. Tel.: +82 63 270 2435; fax: +82 63 270 2306.
E-mail address: shlee66@jbnu.ac.kr (S.-H. Lee).

1566-1199/$ - see front matter © 2011 Elsevier B.V. All rights reserved.
doi:10.1016/j.orgel.2011.11.016

solar energy and solving the global energy crisis and have recently begun to attract large interest as photoactive donor materials in bulk heterojunction organic solar cells [3]. Though still in the early research and development stage, LMW organic semiconductors are promising substitutes for conjugated polymers with substantial potential for generating low cost solar cells devices in the near future due to the simple synthesis, high purity, reproducibility, and low processing cost. With this motivation, continuous efforts have recently been devoted to the creation of new small molecular photoactive materials and their implementation in OSCs applications [4]. In particular, more attention has been paid to the design of small molecules with alternating donor–acceptor (D–A) structures as they can efficiently extend the absorption band through intramolecular charge transfer (ICT) in the D–A systems to better match the solar spectrum and modulate the energy levels to achieve a high power conversion efficiency in solar cells devices. For example, Li et al. described a variety of D–A LMW small molecules based on a triphenylamine (TPA) donor moiety linked to different acceptor moieties, benzothiadiazole (BT), 2-pyran-4-ylidenemalonitrile (PM), and dicyanomethene with linear or star-shaped molecular architectures. The PCE was improved from 0.35% to 1.33% with molecular geometry and the star-shaped material performed better than the linear material [5]. More recently, Li et al. further reported new D–π–A star-shaped molecules using TPA as the core, dicyanovinyl as the end group and acceptor linked with either a bitihophene vinylene π-bridge [6]. These molecules exhibited an absorption band up to 750 nm with a low HOMO level (ca. −5.03 to −5.22) and yielded the best PCE up to 3.0% in the OSC device by blending with $PC_{71}BM$ [6]. Concurrently, Tian et al. demonstrated a series of symmetrical solution-processable small molecules consisting of TPA and PM linked by different electron-donating moieties (phenothiazine, TPA and thiophene) [7]. Through the incorporation of different electron donating moieties, this group provided a method for tuning the optical band gap and energy level of the conjugated system and obtained a PCE in the range of 0.65–1.31% in bulk heterojunction organic solar cells [7c]. Nugyen et al. recently reported a number of LMW-conjugated small molecules based on a diketopyrrolopyole (DPP) pigment core with varied terminal donor segments [8]. By replacing the terminal bithiophene with a benzofuran substituent, they obtained a small molecule that has a deeper HOMO level with high optical density, which yielded high V_{oc} values and a PCE greater than 4% on blending with $PC_{71}BM$ [8d]. A variety of other small molecules that include well-known dye molecules, such as merocyanine [3b,9], squaraine [10], borondipyrromethene [11], and isoindigo [12] have also been reported. By employing a new π-conjugated rigidly fused and planar building block naphtho[1,2-*b*:5,6-*b*′]dithiophene as core and benzothiadiazole or triphenylamine-capped benzothiadiazole as terminal segments, our group has more recently developed novel conjugated small molecules where the PCE up to 2.20% has been achieved [13]. Meanwhile, Zhou et al. have additionally demonstrated a more encouraging PCE of 5.88% by the development of dithienosilole-based conjugated small molecules for solution processed OSCs with preliminary device characterization [14]. Based on all these recent reports, it is now quite evident that the absorption properties, energy levels and charge carrier motilities can also be reasonably tuned to those of efficient conjugated polymers that might soon allow small molecules to deliver a PCE competent to that of polymer solar cells.

Thiazole derivatives, thiophene–bithiazole and thiophene–thiazolothiazole emerged recently as promising acceptors for use in the construction of conjugated polymers. These appear to be very useful semiconductors for both *n*-type and *p*-type organic field effect transistors with high mobilities [15,16]. As high mobility materials are desirable for active components in photovoltaic devices for effective charge transport, many research groups have explored the possible application of thiazole-containing conjugated polymers in the field of bulk heterojunction polymer solar cells. A series of alternating D–A conjugated polymers were synthesized using a bithiazole unit (BTz) with a donor counterpart, including fluorene [17a], carbazole [17b], dithieno[3,2-b:23-d]pyrrole (DTP) [17b], and dithieno[3,2-b:23-d]silole (DTS) [17b]. Of these, the DTS-BTz copolymer demonstrated the best photovoltaic performance with an optimized PCE of 2.86%. Recently, Li et al. reported two new D–A conjugated polymers containing a bezodithiophene (BDT) donor unit and BTz or thiazolothiazole (TTz) acceptor units [18]. Preliminary studies of photovoltaic cells using blends of TTz-based copolymers and $PC_{71}BM$ as the active layer reported an efficiency of 2.60%, while the BTz-based copolymer provided a PCE of 2.03% under identical conditions. In parallel, Shim and co-workers also reported conjugated polymers containing both BTz and TTz units with cyclopentadithiophene (CPDT)-based donors that demonstrated power conversion efficiencies (PCEs) as high as 2.23% under optimized device conditions [19]. In addition, our group also described a TTz-based conjugated copolymer with a didecyloxynaphthalene donor unit with a PCE of approximately 1% [20]. More recently, a TTz and dithienosilole containing conjugated copolymer has demonstrated excellent photovoltaic performance with a PCE of 5.59%, which further suggests that thiazole derivatives could be a promising building block for D–A conjugated copolymers and small molecules [21].

Although, thiazole derivatives have been successfully investigated as comonomers for the synthesis of low band gap D–A conjugated polymers yielding PCEs of ∼0.5–5.6% in polymer solar cells, the application of bithiazole or thiazolothiazole-based small molecules in bulk-heterojunction organic solar cells have not been reported. Therefore, to elucidate their potential in a solution-processable, small molecule organic solar cell, we have designed and synthesized two new conjugated small molecules: 5,5-bis(2-triphenylamino-3-decylthiophen-2-yl)-2,2-bithiazole (**M1**) and 2,5-bis(2-triphenylamino-3-decylthiophen-2-yl)thiazolo[5,4-d]thiazole (**M2**). The small molecules have a D–A–D structure consisting of 5,5-bis(3-decylthiophen-2-yl)-2,2-bithiazole or 2,5-bis(3-decylthiophen-2-yl)thiazolo[5,4-d]thiazole as a central acceptor segment and TPA as a terminal donor segment. The molecules were synthesized using a palladium (0)-catalyzed Suzuki coupling reaction, and the optical and electrochemical properties were compared using UV–vis, photoluminescence (PL), and cyclic voltam-

metry (CV). The photovoltaic performances of the small molecules were investigated by fabricating a bulk heterojunction solar cell device with **M1** or **M2** as the donor and $PC_{61}BM$/$PC_{71}BM$ as the acceptor. The performances of the OSC devices fabricated with **M1** or **M2** were analyzed based on the morphology of the active layer using atomic force microscopy (AFM).

2. Experimental section

2.1. Materials

2-Isopropoxy-4,4,5,5-tetramethyl-1,3,2-dioxaborolane, 3-bromothiophene, dithioxamide, 2-bromothiazole, *n*-butyllithium (2.5 mol/L in hexane), 1,3-bis(diphenylphosphino)propane dichloronickel (II) [Ni(dppp)], 4-(diphenylamino)phenylboronic acid, *N,N*-dimethylformamide (DMF) (anhydrous, 99.8%), *N*-bromosuccinimide (NBS), and 1-bromodecane were purchased from Aldrich. Palladium(II)acetate [$Pd(OAc)_2$], tetrakis(triphenylphosphine)palladium(0) [$Pd(PPh_3)_4$] were obtained from Strem Chemicals. Tetrahydrofuran and diethyl ether were distilled over sodium/benzophenone to maintain the anhydrous condition before use. Chloroform was purified by refluxing with calcium hydride and then distilled. All other chemicals were reagent grade and obtained from commercial sources (Fluka, Across, and TCI) and used as-received without further purification unless stated otherwise. 2-(3-decylthiophen-2-yl)-4,4,5,5-tetramethyl-1,3,2-dioxaborolane (**1**) [22a], 5,5-dibromo-2,2-bithiazole (**2**) [22b], and 3-decylthiophene-2-carboxaldehyde (**8**) [22c] were synthesized following previously reported methods.

2.2. Synthesis of compounds

2.2.1. 5,5-Bis(3-decylthiophen-2-yl)-2,2-bithiazole (3)

5,5-Dibromo-2,2-bithiazole (**2**) (1.11 g, 3.4 mmol), $Pd(PPh_3)_4$ (0.40 g, 0.34 mmol) under a N_2 atmosphere, 30.0 mL of degassed toluene and 10.0 mL of degassed 2 M aqueous K_2CO_3 solution were added to a mixture of 2-(3-decylthiophen-2-yl)-4,4,5,5-tetramethyl-1,3,2-dioxaborolane (**1**) (2.98 g, 8.5 mmol), and the resulting solution was vigorously stirred and heated at reflux for 24 h. When the reaction was completed, water was added to quench the reaction. The product was extracted with dichloromethane (CH_2Cl_2). The organic layer was collected, dried over anhydrous $MgSO_4$ and evaporated under reduced pressure. The resulting crude product was adsorbed on silica gel and purified by column chromatography using a hexane/CH_2Cl_2 mixture (4:1) as the eluent to produce **3** (1.08 g, 64%) as a dark yellow solid. **^{1}H NMR** (400 MHz, $CDCl_3$, ppm) δ: 7.84 (s, 2H), 7.24–7.21 (d, 2H), 6.95–6.93 (d, 2H), 2.72 (t, 4H), 1.58 (q, 4H), 1.33–1.22 (m, 28H), 0.84 (t, 6H). **^{13}C NMR** ($CDCl_3$, 100 MHz, ppm) δ: 160.23, 141.92, 141.30, 133.44, 130.25, 126.04, 125.32, 31.91, 30.53, 29.62, 29.53, 29.50, 29.49, 22.59, 14.12. **Elemental analysis**: Calculated for $C_{34}H_{48}N_2S_4$: C, 66.62%; H, 7.89%; S, 20.92%. Found: C, 65.98%; H, 7.96%; S, 20.84%.

2.2.2. 5,5-Bis(5-bromo-3-decylthiophen-2-yl)-2,2-bithiazole (4)

5,5-Bis(3-decylthiophene-2-yl)-2,2-bithiazole (**3**) (0.8 g, 1.3 mmol) was dissolved in a mixture of chloroform (7.5 mL) and glacial acetic acid (7.5 mL). NBS (0.48 g, 2.73 mmol) was added drop-wise to the solution and stirred in the dark for an hour. The reaction mixture was subsequently hydrolyzed with water and extracted with dichloromethane. The organic layer was washed three times with 40 mL water and dried over magnesium sulfate. The residue obtained via solvent evaporation was purified using column chromatography with silica gel (eluent: hexane/CH_2Cl_2 = 5:1 v/v) to produce product **4** as a yellow solid (0.72 g, 72%). **^{1}H NMR** (400 MHz, $CDCl_3$, ppm) δ: 7.80 (s, 2H), 6.95 (s, 2H), 2.69 (t, 4H), 1.58 (q, 4H), 1.25 (m, 28H), 0.87 (t, 6H). **^{13}C NMR** ($CDCl_3$, 100 MHz, ppm) δ: 160.43, 142.62, 141.70, 132.88, 132.25, 127.34, 112.43, 31.87, 30.41, 29.56, 29.50, 29.38, 29.29, 22.65, 14.1. **Elemental analysis**: Calculated for $C_{34}H_{46}Br_2N_2S_4$: C, 52.98%; H, 6.02%; S, 16.64%. Found: C, 52.87%; H, 6.11%; S, 16.58%.

2.2.3. 2,5-Bis(3-decylthiophen-2-yl)thiazolo[5,4-d]thiazole (9)

A solution of 3-decylthiophene-2-carboxaldehyde (**8**) (3.4 g, 13.5 mmol) and dithiooxamide (0.735 g, 6.13 mmol) in *N,N*-dimethylformamide (30 mL) was heated under reflux for 6 h and cooled to room temperature. The reaction mixture was poured into water and extracted with methylene chloride. The organic layer was washed three times with water and dried over anhydrous magnesium sulfate. The solvent was evaporated, and the brown residue was purified via column chromatography using silica gel (eluent: hexane/dicholoromethane = 5:1 v/v) to produce the product (yield = 22%). **^{1}H NMR** (400 MHz, $CDCl_3$, ppm) δ: 7.36 (d, J = 5.1 Hz, 2H), 7.04 (d, J = 5.1 Hz, 2H), 2.98 (t, J = 7.6 Hz, 4H), 1.71 (q, J = 7.8 Hz, 4H), 1.29 (br, 28H), 0.90 (t, J = 6.7 Hz, 6H). **^{13}C NMR** ($CDCl_3$, 100 MHz, ppm) δ: 161.6, 150.0, 143.1, 131.8, 130.8, 127.3, 31.92, 30.4, 30.1, 30.0, 29.6, 29.5, 29.4, 22.7, 14.1. **Elemental analysis**: Calculated for $C_{32}H_{46}N_2S_4$: C, 65.48%; H, 7.9%; S, 21.85%. Found: C, 65.5%; H, 7.75%; S, 21.92%.

2.2.4. 2,5-Bis(5-bromo-3-decylthiophen-2-yl)thiazolo[5,4-d]thiazole (10)

2,5-Bis(3-decylthiophen-2-yl)thiazolo[5,4-d]thiazole (**9**) (2 gm, 3.4 mmol) was dissolved in a mixture of chloroform (20 mL) and glacial acetic acid (20 mL). NBS (1.33 g, 7.5 mmol) was added drop-wise to the solution and stirred in the dark for an hour. The reaction mixture was subsequently hydrolyzed with water and extracted with dichloromethane. The organic layer was washed three times with 100 mL water and dried over magnesium sulfate. The residue obtained via solvent evaporation was purified using column chromatography with silica gel (eluent: hexane/dichloromethane = 5:1 v/v) to produce a yellow solid product. (yield = 75%). **^{1}H NMR** (400 MHz, $CDCl_3$, ppm) δ: 6.88 (s, 2H), 2.81 (t, J = 7.6 Hz, 4H), 1.61 (q, 4H), 1.20 (br, 28H), 0.81 (t, J = 7.2 Hz, 6H). **^{13}C NMR** (Fig. S6) ($CDCl_3$, 100 MHz, ppm) δ: 160.3, 150.0, 143.4, 133.4, 115.4, 31.9, 30.2, 29.8, 29.7, 29.6, 29.4, 29.3, 22.7, 14.1. **Elemental analysis:** Calculated for $C_{32}H_{44}Br_2N_2S_4$: C, 51.61; H, 5.95; S, 17.22. Found: C, 51.7; H, 5.88; S, 17.12.

2.2.5. 5,5-Bis(2-triphenylamino-3-decylthiophene-2-yl)-2,2-bithiazole (M1)

In a 50 mL flame-dried two neck flask, 5,5-bis(5-bromo-3-decylthiophene-2-yl)-2,2-bithiazole (**4**) (0.3 g,

0.39 mmol), 4-(diphenylamino)phenylboronic acid (**11**) (0.28 g, 0.97 mmol), and $Pd(PPh_3)_4$ (40 mg, 10 mol%) were added and subjected to three vacuum/nitrogen fill cycles. Nitrogen-degassed toluene (12 mL) and an aqueous 2 M K_2CO_3 solution (4 mL) were subsequently added. The reaction mixture was heated to reflux for 24 h and was monitored by TLC. After completion, water was added to quench the reaction and the organic layer was extracted with dichloromethane. The dichloromethane was subsequently removed under reduced pressure. The resulting crude product was purified by column chromatography eluting with hexane/CH_2Cl_2 (4:1) to produce the target compound **M1** as a red solid (0.28 g, 67%). **^{1}H NMR** (400 MHz, $CDCl_3$, ppm) δ: 7.87 (s, 2H, ArH), 7.45–7.26 (dd, 8H, ArH), 7.26–7.08 (dd, 4H, ArH), 7.12–7.02 (dd, 16H, ArH), 7.04 (s, 2H, ArH) 2.78 (t, 4H), 1.69–1.64 (m, 4H), 1.40–1.25 (m, 28 H), 0.87 (t, 6H). **^{13}C NMR** ($CDCl_3$, 100 MHz, ppm) δ: 159.69, 147.70, 147.32, 143.62, 142.81, 140.89, 133.61, 129.32, 127.38, 126.46, 125.25, 124.71, 124.65, 123.31, 123.27, 31.87, 30.42, 29.78, 29.67, 29.58, 29.52, 29.48, 29.30, 22.65, 14.09. **Elemental analysis**: Calculated for $C_{70}H_{74}N_4S_4$, C, 76.46%; H, 6.78%; S, 11.66%. Found: C, 76.43%; H, 6.82%; S, 11.71%.

2.2.6. 2,5-Bis(2-triphenylamino-3-decylthiophen-2-yl)thiazolo[5,4-d]thiazole (M2)

2,5-Bis(2-triphenylamino-3-decylthiophen-2-yl)thiazol o[5,4-d] thiazole (**M2**) was prepared using a method simil ar to that reported for compound **M1**. Briefly, a mixture of 2,5-bis(3-decylthiophen-2-yl)thiazolo[5,4-d]thiazole (**9**) (0 .24 g , 0.32 mmol), 4-(diphenylamino)phenylboronic acid (**11**) (0.23 g, 0.80 mmol) and $Pd(PPh_3)_4$ (30 mg, 10 m ol%) were refluxed in nitrogen-degassed toluene (12 mL) and an aqueous 2 M K_2CO_3 solution (4 mL) to yield 0.21 g (63%) of **M2** as a red solid. **^{1}H NMR** (400 MHz, $CDCl_3$, ppm) δ: 7.47–7.25 (dd, 8H, ArH), 7.25–7.1 (dd, 4H, ArH), 7.12–7.02 (dd, 16H, ArH), 7.04 (s, 2H, ArH) 2.89 (t, 4H), 1.75–1.70 (m, 4H), 1.45–1.26 (m, 28 H), 0.87 (t, 6H). **^{13}C NMR** ($CDCl_3$, 100 MHz, ppm) δ: 160.99, 149.84, 147.88, 147.29, 147.21, 145.34, 143.99, 130.13, 129.66, 129.32, 127.12, 126.46, 125.55, 124.86, 124.74, 123.34, 123.03, 122.56, 31.87, 30.46, 29.81, 29.68, 29.60, 29.45, 29.32, 22.65, 14.10. **Elemental analysis**: Calculated for $C_{70}H_{74}N_4S_4$, C, 76.46%; H, 6.78%; S, 11.66%. Found: C, 76.43%; H, 6.82%; S, 11.71%.

2.3. General instrumentation

The ^{1}H and ^{13}C NMR spectra were recorded on a JEOL FT-NMR (400 MHz) spectrophotometer using $CDCl_3$ as a solvent. Chemical shifts were reported as δ values (ppm) relative to tetramethylsilane (TMS) as internal standards. Elemental analyses were performed using CE Instruments Flash EA 1112 series. UV–Vis absorption spectra were obtained using a Shimadzu UV-2550 spectrophotometer. Photoluminescence (PL) spectra of films or solutions in chloroform were obtained using a FP-6500 (JASCO). Differential scanning calorimetry (DSC) was performed on a TA instrument (DSC 2910) at a heating rate of 15 °C min^{-1} under a nitrogen atmosphere. Cyclic voltammetry (CV) measurements were performed on a VersaSTAT3 (METEK) using a solution of tetrabutylammonium hexafluorophosphate (n-Bu_4NPF_6) (0.10 M) in acetonitrile, under argon, at a scan rate of 50 mV s^{-1} at room temperature. A Pt wire and Ag/AgCl were used as the counter and reference electrodes, respectively. The surface morphology was measured using an atomic force microscope (AFM, Digital Instruments, tapping mode).

2.4. Photovoltaic device fabrication and characterization

The organic photovoltaic cells were prepared on a commercial ITO-coated glass substrate with a sandwiched structure of glass/ITO/PEDOT:PSS/**M1** or **M2**:$PC_{61}BM$ and $PC_{71}BM$/LiF/Al with an active area of 9 mm^2. Prior to use, the patterned ITO glass was cleaned with deionized water, acetone, and isopropyl alcohol using ultrasonication, followed by treatment with UV and O_3. The PEDOT:PSS (AI 4083, H.C. Starck) was spin-coated (2600 rpm, 40 s) onto the ITO glass at a thickness of 40 nm and dried at 140 °C for 20 min. Blends of **M1** or **M2** and $PC_{61}BM$ or $PC_{71}BM$ (Nano-C, USA) with different weight ratios (from 1:1 to 1:4 w/w) was solubilized overnight in chloroform or chlorobenzene, filtered through a 0.45-μm poly(tetrafluoroethylene) (PTFE) filter and subsequently spin-coated at 1000–3000 rpm for 60 s (thickness, 60–95 nm) onto the PEDOT:PSS layer of the ITO. The resulting films were dried at RT for 20 min under nitrogen and then under vacuum at room temperature for 12 h. The devices were completed by deposition of a 0.5-nm layer of LiF and a 120-nm Al layer. The current–voltage (J–V) characteristics of the photovoltaic devices were measured in the dark and under white light illumination at AM 1.5G using a solar simulator (Newport) at 100 mW/cm^2, adjusted with a standard PV reference (2 × 2 cm), a mono-crystalline silicon solar cell (calibrated at NREL, Colorado, USA) with a Keithley 2400 source-measure unit. The external quantum efficiency (EQE) was determined using a Polaronix K3100 spectrometer.

3. Results and discussion

3.1. Synthesis and structural characterization

The syntheses of the small molecules **M1** and **M2** are outlined in Scheme 1. Decylthiophene–capped-bithiazole (**3**) was prepared using a Suzuki coupling reaction between **1** and **2** with $Pd(PPh_3)_4$ as a catalyst. Compound **8** was reacted with dithioxamide to prepare the thiazolothiazole derivative (**9**) with slight modification of the procedure reported by McCullough et al. [15c]. Both **3** and **9** were brominated with NBS to produce the bromine functionalized bithiazole (**4**) and thiazolothiazole (**10**) derivatives. Finally, a $Pd(PPh_3)_4$-catalyzed Suzuki coupling reaction between **11** and **4** or **10** produced the target small molecules, **M1** and **M2**. The small molecules and intermediate compounds were characterized using ^{1}H-NMR, ^{13}C-NMR, and elemental analysis. DSC measurements were performed to determine the molecular transition of the small molecules. However, no glass transition or melting was observed, which suggests that these small molecules are amorphous in nature.

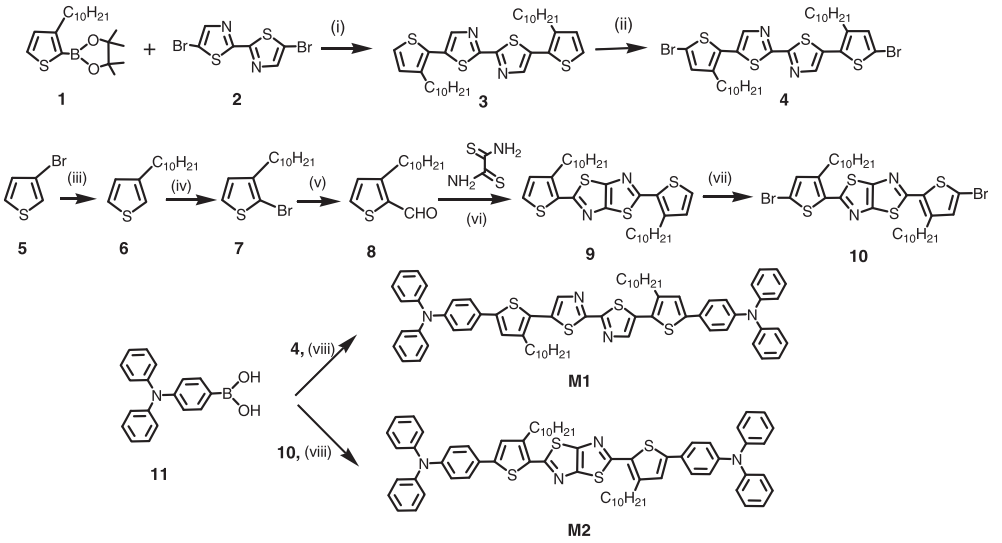

Scheme 1. Synthetic route to produce the small molecules. Reagents and conditions: (i) $Pd(PPh_3)_4$, K_2CO_3, toluene, reflux; (ii) NBS, $CHCl_3$/AcOH; (iii) Ni(dppp), ether, $C_{10}H_{21}MgBr$; (iv) NBS, DMF, room temperature, 12 h; (v) *n*-BuLi, DMF, THF, −78 °C; (vi) DMF, reflux, 5 h; (vii) NBS, $CHCl_3$/AcOH; (viii) $Pd(PPh_3)_4$, K_2CO_3, toluene.

Table 1
The optical and electrochemical properties of small molecules.

Small molecule	λ_{max} (nm), chloroform		[a]E_g^{opt} (eV)	[b]E_{ox}/[c]HOMO (eV)	[d]LUMO (eV)
	Solution	Film			
M1	452	462	2.22	0.87/−5.27	−3.05
M2	465	469	2.25	0.92/−5.32	−3.07

[a] $E_g^{opt} = 1240/(\lambda_{onset})_{film}$.
[b] Potential determined by cyclic voltammetry in 0.10 M Bu_4NPF_6–CH_3CN vs. Ag/AgCl.
[c] HOMO = $-e(4.4 + E_{onset}^{ox})$ (eV).
[d] LUMO = E_g^{opt} + HOMO.

3.2. Optical properties

The UV–visible absorption spectra of the small molecules were measured at room temperature both in dilute (10^{-5} M) chloroform solutions and in spin coated thin films. The corresponding absorption data are summarized in Table 1. Fig. 1 presents the normalized UV–Vis spectra of both **M1** and **M2** in chloroform and as a cast thin film. The **M1** in chloroform solution showed absorption band in the range of 300–550 nm with an absorption maximum (λ_{max}) at 452 nm. The **M2** also exhibited an absorption band in the range of 300–550 nm, however, the λ_{max} of **M2** was located at 465 nm, which was 13 nm red shifted in comparison with that of the **M1** in solution. In addition, at 465 nm, the molar extinction coefficient of **M2** (53,000 L $M^{-1}cm^{-1}$) was higher than that of **M1** (39,800 L $M^{-1}cm^{-1}$). The small molecules have a D–A–D structure in which the terminal donor (D) segments are same (triphenyl amine), while they differ only at the acceptor (A) counterpart, i.e. bithiazole in case of **M1** and thiazolothiazole in case of **M2**. In general, using the same donor unit with varying only at the acceptor counterpart, the optical properties of a D–A conjugated small molecule depend on the strength of the acceptor. The stronger the electron-withdrawing ability of the acceptor, higher is the electron delocalization degree and stronger is the intermolecular charge transfer transition. However, in the present case, since, both **M1** and **M2** have same electron–withdrawing imine (–C=N) groups in the respective thiazole units, the difference in the electron withdrawing ability of thiazolothiazole or bithiazole units are supposed to have negligible effect in the difference of the optical properties of the small molecules, which is quite evident by the similar absorption patterns of **M1** and **M2**. However, the small difference as revealed in the absorption maxima and molar extinction coefficient can be attributed to the different structural arrangement of the small molecules, as it is widely known that planar structure also makes a difference in the effective conjugation length and absorption properties than those with non-planar structure. More specifically, unlike **M1**, which contains two thiazole rings connected through a single bond, **M2** possesses two thiazole rings fused in the core, which is likely to enhance the coplanarity of the **M2** molecule, extend the conjugation length and consequently cause a slight red-shifted absorption maxima and a higher molar extinction coefficient [18,21,23–26]. A comparison of the thin film absorption spectra of the small molecules further revealed that **M2** ($\Delta\lambda$ (λ_{max} (solid) − λ_{max} (solution) ∼ 4 nm) had a slightly less red shifted λ_{max} than **M1** ($\Delta\lambda \sim 10$ nm) as compared to when in solution, thus indicating **M2** to be comparatively more aggregated even in solution. In other words, a substantial amount of interchain electronic delocalization was already achieved in solution for **M2** due to its more planar thiazolothiazole unit. The optical band gap (E_g^{opt}) of **M1** calculated from the absorption edge was 2.22 eV, which was slightly (0.03 eV) less than that of **M2**. The E_g^{opt} values of the present small molecules were higher (∼0.05–0.07 eV) than the triphenylamine–benzothiadiazole (TPA–BT) containing analogous small molecule reported by Zhan and co workers [27], which can be

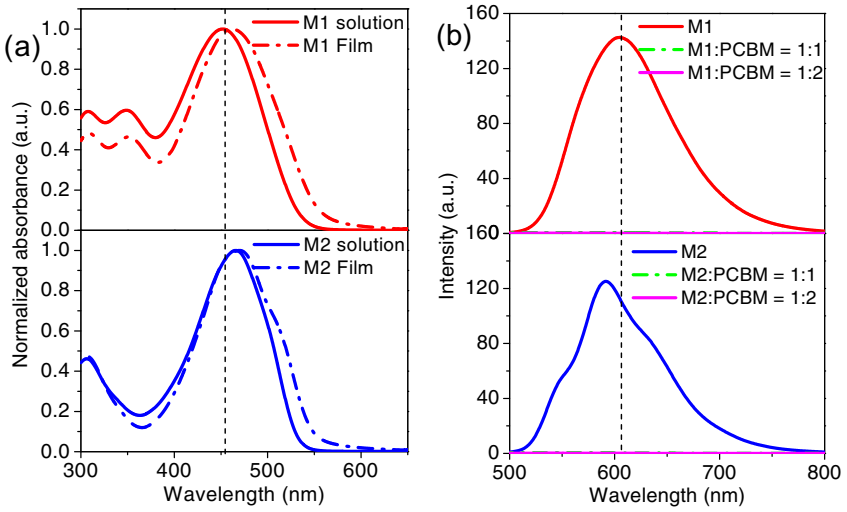

Fig. 1. (a) Normalized UV–vis absorption spectra of **M1** and **M2** in chloroform (1×10^{-5} M) and as thin films at room temperature; (b) Photoluminescence spectra of **M1**, **M2** and **M1** or **M2**/$PC_{61}BM$-blended films.

explained by the weaker electron withdrawing ability of bithiazole or thiazolothiazole units compared to bezothiadiazole counterpart. As the band gap of the donor materials is the difference between the HOMO and LUMO energy levels, the relatively higher band gap of **M1** and **M2** may produce a low lying HOMO value which in turn facilitates the improvement in the photovoltage of the solar cell devices.

PL spectra of the small molecules and small molecules blended with PCBM were examined for the charge transfer process from small molecules to PCBM. Fig. 1b compares the PL spectra of **M1**, **M2**, and **M1** or **M2**/$PC_{61}BM$ composite in solid thin film states with different weight ratios (1:0, 1:1, and 1:2). **M1** showed a strong PL emission band with emission maxima at 604 nm, whereas **M2** exhibited an emission band at 591 nm, which was blue-shifted 13 nm compared to that of **M1**. Upon addition of PCBM, the emission bands for both **M1** and **M2** were nearly quenched, even with 1:1 (w/w) blend ratio, indicating an effective charge transfer process between the small molecules and PCBM.

3.3. Electrochemical properties

In order to evaluate the electrochemical properties of the small molecules, CV was performed in a 0.1 M solution of Bu_4NPF_6 in acetonitrile at room temperature under argon with a scan rate of 50 mV s^{-1}. The CV curves were recorded referenced to Ag/AgCl reference electrode, which was calibrated using ferrocene/ferrocenium (Fc/Fc^+) redox couple (4.4 eV below the vacuum level) as an external standard. The cyclic voltammogram of **M1** and **M2** are displayed in Fig. 2a. On the anodic sweep, **M1** exhibited a slightly reversible oxidation peak with onset potentials (E^{ox}_{onset}) of 0.87 V (versus Ag/AgCl), while **M2** showed a completely irreversible peak with onset oxidation potentials of 0.92 V. The HOMO energy levels of the small molecules were determined to be −5.27 eV, for **M1** and −5.32 eV for **M2** from the corresponding E^{ox}_{onset} according to the following equation: $E_{HOMO} = -e(E^{ox}_{onset} + 4.4)$ (eV) [28]. Based on the correlation between the HOMO energy level and E^{opt}_g, estimated from the UV–Vis absorption spectrum of the film samples ($E_g = E_{HOMO} - E_{LUMO}$), the LUMO energy levels of **M1** and **M2** were calculated to be −3.05 eV and −3.07 eV, respectively. The results of the electrochemical measurements and calculated energy levels of the small molecules are further listed in Table 1. By comparing the energy levels in Table 1, it appeared that though there is slight difference (0.05 eV) in the HOMO energy levels of the small molecules, the LUMO energy levels of **M1** and **M2** remained almost invariant. Since, the LUMO level is mainly delocalized in the acceptor counterpart, the unaffected LUMO energy levels for the small molecules indicating that both the acceptor bithiazole and thiazolothiazole contributed almost similar electron-deficient character in the D–A–D conjugated unit, which additionally support our discussion with the optical properties of the small molecules in the previous section. The small difference in HOMO value of **M1** compared to **M2** could be explained by the reduction in band gap of **M1**. It is further important to note that the oxidation potential of both **M1** and **M2** is greater than that of regioregular poly(3-hexylthiophene) (rrP3HT) [29], which indicates that the present small molecules have better oxidative stability as compared to rrP3HT. In addition, the LUMO energy levels of the small molecules (**M1** and **M2**) are well-aligned with the LUMO levels of PCBMs [30a] (Fig. 2b) with energy difference >0.3 eV, indicating that the generated excitons can efficiently be dissociated at the interface between small molecules and PCBM [30b]. The HOMO energy levels of **M1** and **M2** are less (0.07–0.12 eV) than that of the analogous small molecules based on TPA–BT [27]. Since the V_{oc} of OSC is determined by the difference between the HOMO level of the donor and the LUMO of the acceptor, the HOMO energy level of the related donor molecules in a bulk-heterojunction photovoltaic cell is very important for a high efficiency device [31,32]. Obviously, it is expected that with a

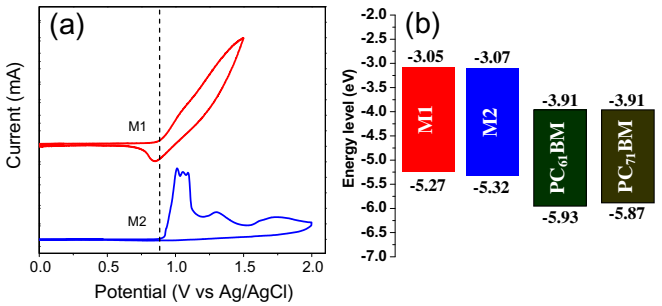

Fig. 2. (a) Cyclic voltammogram of **M1** and **M2** films on a platinum electrode in a 0.1 mol L^{-1} Bu_4NPF_6 CH_3CN solution at a scan rate of 50 mV/s. (b) The HOMO and LUMO energy levels of the small molecules and PCBMs.

relatively low HOMO level (−5.27 to −5.32 eV) compared with P3HT (HOMO = −4.76 eV) [29] or TPA–BT small molecule (HOMO = −5.2) [27], our newly synthesized small molecules may favor for the improvement of the V_{oc} on construction of the photovoltaic cells with PCBM as acceptor.

3.4. Photovoltaic properties

To explore the photovoltaic performance of the small molecules, bulk heterojunction OSCs were fabricated using **M1** and **M2** as the donor and fullerene derivatives, $PC_{61}BM$ or $PC_{71}BM$ as the acceptor with device architecture ITO/PEDOT:PSS/**M1** or **M2**:$PC_{61}BM$ or $PC_{71}BM$/LiF/Al. During the preliminary device optimization process, we fabricated cells with different small molecule/$PC_{61}BM$ weight ratios (from 1:1 to 1:4) at an active layer thickness of 80–85 nm (a spin-coating rate of 1000 rpm for 60 s) from chloroform solution. All devices were tested in the dark and under illumination of AM 1.5G (100 mW/cm^2). The typical current density–voltage (J–V) characteristics of the related solar cell devices are presented in the Supporting Information (Fig. S9). The corresponding short circuit current (J_{sc}), open circuit voltage (V_{oc}), fill factor (FF), and power conversion efficiency (PCE) of the devices are summarized in Table 2. Optimal fabrication conditions were achieved using a small molecule-to-$PC_{61}BM$ ratio of 1:3 (w/w) for both **M1** and **M2**. The device with a 1:3 weight ratio of **M1** to $PC_{61}BM$ provided a V_{oc} of 0.72 V, a J_{sc} of 2.42 mA cm^{-2}, and FF of 0.42, resulting in an estimated PCE of 0.74%. In contrast, the device based on **M2** and $PC_{61}BM$ with the same weight ratio delivered a slightly improved performance with a V_{oc} of 0.92 V, a J_{sc} of 2.79 mA cm^{-2}, and an FF of 0.32, yielding a PCE of 0.81%. Because of the similar absorption profile, both the small molecules produced a similar J_{sc} in the solar cell devices. However, the V_{oc} of the photovoltaic devices based on **M1**/$PC_{61}BM$ were less than that of the **M2**/$PC_{61}BM$ devices, despite their similar HOMO level, which attributed to the different device morphology as discussed later.

$PC_{71}BM$ has more absorption in the visible region than $PC_{61}BM$ [33]. Therefore, at identical device conditions, $PC_{71}BM$ may contribute to more current from the device and may provide a means to enhance the device efficiency. In order to determine if the performances of the small molecules could be further improved with $PC_{71}BM$, we also fabricated a series of devices using $PC_{71}BM$ as the acceptor. The small molecule to $PC_{71}BM$ ratio was fixed at 1:3 and the active layer was coated from a chloroform solution at a thickness of ~80–85 nm, as this condition was optimal for $PC_{61}BM$. The device results are listed in Table 2. Indeed, after changing the electron acceptor from $PC_{61}BM$ to $PC_{71}BM$, a higher J_{sc} value was obtained for both **M1** and **M2** devices due to the higher absorption coefficient of $PC_{71}BM$ in the visible region [34–36]. More interestingly, a dramatic increase in J_{sc} was observed from 2.79 to 6.36 mA cm^{-2} for **M2**, which was much larger than that of **M1**. The J_{sc} strongly depends on the number of excitons generated in the photoactive layers and their dissociation into free charge carriers at the interfaces, which is directly related to the optical absorption properties of the photoactive layers. Although the small molecules **M1** and **M2** have a similar E_g with a gap difference of 0.03 eV, **M2** has a stronger absorption with 1.33 times higher molar absorptivity (at longer wavelength ~ 465 nm) than **M1**, which plausibly contributed to more excitons and charge generation in the **M2**/$PC_{71}BM$ device than in the **M1**/$PC_{71}BM$ device. The larger number of generated excitons is likely one of the main reasons for the enhanced J_{sc} in the **M2**/$PC_{71}BM$ devices. However, the effect of differences in charge carrier mobility cannot be ruled out [37]. More specifically, because of a more planar structure, charge transport is expected to be better-facilitated in **M2**/PCBM devices than in **M1**/PCBM devices, which could be an alternative reason for the enhanced J_{sc} in the **M2**/$PC_{71}BM$-based

Table 2
Summary of photovoltaic performances of the OSCs based on **M1** and **M2**:PCBM blends with different weight ratio in chloroform with active layer thickness 80–85 nm.

Active layer	J_{sc} (mA cm^{-2})	V_{oc} (V)	FF	PCE (%)
M1:$PC_{61}BM$ = 1:1	1.77	0.77	0.34	0.46
M1:$PC_{61}BM$ = 1:2	1.56	0.69	0.36	0.39
M1:$PC_{61}BM$ = 1:3	2.42	0.72	0.42	0.74
M1:$PC_{61}BM$ = 1:4	1.31	0.68	0.39	0.35
M1:$PC_{71}BM$ = 1:3	4.05	0.94	0.27	1.03
M2:$PC_{61}BM$ = 1:1	1.45	0.94	0.27	0.37
M2:$PC_{61}BM$ = 1:2	2.52	0.92	0.32	0.75
M2:$PC_{61}BM$ = 1:3	2.79	0.92	0.32	0.81
M2:$PC_{61}BM$ = 1:4	2.52	0.92	0.30	0.70
M2:$PC_{71}BM$ = 1:3	6.36	0.92	0.35	2.05

devices. In fact, a higher hole mobility was also observed earlier for TTz-based conjugated polymers compared to that of the corresponding BTz copolymer due to the highly rigid and planar thiazolothiazole unit in the backbone, which enhanced the π–π intermolecular stacking [18,26]. In addition to J_{sc}, the V_{oc} for the **M1**/$PC_{71}BM$ cell was greatly improved from 0.72 to 0.94 V; however such an improvement was not observed for **M2**/$PC_{71}BM$ cells, but a steady value of V_{oc} (0.92 V) was obtained. With the increased J_{sc}, the PCE of **M1** increased from 0.7% to 1.03%, while the PCE increased from 0.81 to 2.05% for **M2**, which is approximately a 2.5-fold increase over the device based on **M2**/$PC_{61}BM$.

In addition to two different PCBM qualities, the variation of solvent was also considered for further improvement of the device performance. The choice of solvent can greatly affect the morphology of the active layers and thus influence the overall device performance [38,39]. Several other groups have systematically investigated the effect of solvents on the morphology of small molecules and in many cases, chlorobenzene was proven to be a better solvent for achieving higher photovoltaic performance [7c,36,40,41]. Therefore, in our study, in addition to chloroform, we also fabricated cells with active layers processed from chlorobenzene while maintaining the weight ratio of small molecules:$PC_{71}BM$ at 1:3. However, the thickness of the active layers varied within the range of 65–95 nm by changing both the spinning speed and concentration of the active layer solution to optimize the active layer thickness. Fig. 3a displays the *J*–*V* curves of representative cells prepared from small molecule blends with $PC_{71}BM$. The solar cell device parameters are summarized in Table 3. The **M1**:$PC_{71}BM$ device (1:3 w/w) with an active layer thickness of approximately 65 nm had a V_{oc} of 0.97 V, a J_{sc} of 4.63 mA cm^{-2}, and FF of 0.29, resulting in an estimated PCE of 1.30%. For **M2**, the device with a **M2**:$PC_{71}BM$ (1:3 w/w) and active layer thickness of approximately 75 nm exhibited the best PCE of 2.39% with a V_{oc} of 0.94 V, a J_{sc} of 6.49 mA cm^{-2}, and FF of 0.39. By changing the processing solvent from chloroform to chlorobenzene, all three device parameters (V_{oc}, J_{sc}, and FF) for both **M1**/$PC_{71}BM$ and **M2**/$PC_{71}BM$ solar cell devices slightly improved, and this improvement may have resulted from better device morphology.

When comparing the performance of our **M2**/$PC_{71}BM$ device with that of the device based on an analogous small molecule, TPA–BT, and $PC_{71}BM$ reported by Zhan et al., the present device exhibits a 2.81 mA/cm^2 higher J_{sc} and a 0.08 V larger V_{oc} than that of the TPA–BT/$PC_{71}BM$ device and as a consequence, a 1.16% higher PCE value. Fig. 3(b) compares the EQE of **M1**/$PC_{71}BM$ (1:3 w/w) and **M2**/$PC_{71}BM$ (1:3 w/w) devices fabricated from the chlorobenzene solution together with as cast composite film absorption. Both devices exhibited photon to current conversion efficiency in the range of 300 to 700 nm, which corroborates the corresponding absorbance spectra and thus suggests that most of the absorptive photons are converted into a photocurrent. The **M1**/$PC_{71}BM$ device exhibited a maximum EQE over 30% in the range of 380 to 520 nm. In comparison, the **M2**/$PC_{71}BM$ showed a broader and higher EQE with a maximum efficiency of 50% at 380 nm and 46% at 480 nm.

3.5. Device morphology

To gain a better understanding of what may be controlling the different photovoltaic performances of the small molecules, AFM measurements were performed to examine the surface morphology of the **M1** or **M2**/PCBM composite films under different conditions. Fig. 4a and b show AFM topography and phase images of **M1**:$PC_{61}BM$ (1:3 w/w) and **M2**:$PC_{61}BM$ (1:3 w/w) blended films cast from chloroform. **M1** had poor miscibility with $PC_{61}BM$, resulting in large phase segregated domains throughout the surfaces. In comparison, regardless of their structural similarity, **M2** was more compatible with $PC_{61}BM$, leading to smaller **M2** and $PC_{61}BM$ (rms 0.74) aggregated domains in the matrix and lower surface roughness compared to the **M1**:$PC_{61}BM$ blend film (rms 1.36 nm). The increased phase segregated domains and higher roughness induced a decrease in the D/A interfacial area for efficient charge separation and transport, resulting in both lower J_{sc} and lower V_{oc} values in the **M1**/$PC_{61}BM$ devices as shown in Table 3. On replacement of $PC_{61}BM$ with $PC_{71}BM$ in **M1**/$PC_{71}BM$ (Fig. 4c) and **M2**/$PC_{71}BM$ (Fig. 4d) films, the number of phase-segregated domains was reduced and the surface morphology appeared to improve significantly, suggesting that **M1** and **M2** are more miscible with $PC_{71}BM$ compared to $PC_{61}BM$. Moreover, the **M2**/$PC_{71}BM$ film exhibited relatively smoother morphology with homogeneous distribution of **M2** and $PC_{71}BM$ (rms 0.24 nm), which accounts for its better photovoltaic performance compared to that of the **M1**:$PC_{71}BM$ device. When comparing the AFM images of **M1**:$PC_{71}BM$ (Fig. 4e) and **M2**:$PC_{71}BM$ (Fig. 4f) films coated from the chlorobenzene solution to that of films from chloroform (Fig. 4c and d), not much improvement in morphology was observed and the surface roughness remained nearly the same. However, more intimate mixing with a decreasing domain size of **M1** or **M2** and $PC_{71}BM$ occurred, which could partially explain the slightly improved device performance compared to the device processed from the chloroform solution.

4. Conclusions

In summary, we designed, synthesized and characterized two novel small molecules **M1** and **M2** based on thiophene–bithiazole and thiophene–thiazolothiazole acceptors, respectively, with a D-A-D type molecular structure. These small molecules had very similar optical band gaps (2.22–2.25 eV) and fairly close HOMO energy levels (−5.27 to −5.32 eV). The best BHJ solar cells using **M2** as a donor and $PC_{71}BM$ as an acceptor demonstrated efficient device performance with a noticeably high V_{oc} of 0.94 V and a PCE of nearly 2.4%. The OSC based on **M1** and $PC_{71}BM$ exhibited an even higher V_{oc} of 0.97 V under optimized conditions, however the device efficiency was relatively low (1.30%) with a low J_{sc} due to suboptimal film morphology and poor charge transport capability. Though, as a consequence of our simple, rational, and straightforward synthetic design we could achieve the HOMO value of one of the small molecules, **M2** (−5.32 eV) very close to the proposed ideal HOMO value of −5.4 eV [32] resulting in a notably high V_{oc}, the PCE

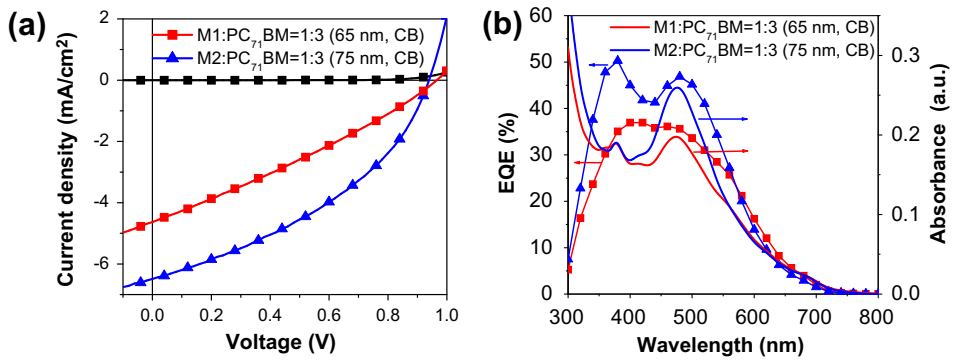

Fig. 3. (a) *J–V* curves for small molecule:$PC_{71}BM$ solar cell devices at a 1:3 w/w ratio in chlorobenzene under an illumination of AM 1.5G and 100 mW/cm^2. (b) EQE of the solar cell devices and absorbance spectra of the as-cast thin film of the small molecule:$PC_{71}BM$ composites at a 1:3 w/w ratio in chlorobenzene.

Table 3
Photovoltaic performances of the OSCs based on **M1** and **M2**:$PC_{71}BM$ blends (1:3 w/w) with different active layer thickness processed from chlorobenzene solvent.

Active layer	Thickness	J_{sc} (mA cm^{-2})	V_{oc} (V)	FF	PCE (%)
M1:$PC_{71}BM$	92	2.69	0.72	0.29	0.55
M1:$PC_{71}BM$	84	4.44	0.78	0.31	1.05
M1:$PC_{71}BM$	72	4.88	0.76	0.32	1.19
M1:$PC_{71}BM$	65	4.63	0.97	0.29	1.30
M2:$PC_{71}BM$	89	6.32	0.94	0.37	2.19
M2:$PC_{71}BM$	83	6.57	0.94	0.38	2.37
M2:$PC_{71}BM$	75	6.49	0.94	0.39	2.39
M2:$PC_{71}BM$	67	6.31	0.94	0.40	2.38

is moderate due to not obtaining optimal J_{sc} sacrificing in desired low band gap. Therefore, a still stronger donor unit is required to combine with these thiazole units to bathochormically tune the absorption band for better matching the solar spectrum with parallel modulation to the optimal HOMO–LUMO levels. The synthesis could be extended as D–A–D, A–D–A, and more extended D–A molecular structures with these thiazole acceptors employing rigidly fused multicyclic planar building block such as dithieno[3,2-b:23-d]silole, benzo[1,2-b:4,5-b]dithiophene as π-conjugated donors. This would make the molecular back bone more rigid and coplanar therefore enhancing effective π-conjugation, extending absorption, and lowering band gap, and consequently, would facilitate charge carrier mobility that might significantly improve the device performance. It would be also interesting to see the properties of the small molecules if the present bithiazole unit is replaced with the bithiazole unit having two N atoms pointing outwards. Nevertheless, based on our preliminary photovoltaic studies, it can be concluded that besides DPP, BT, and PM, the thiazole derivatives, BTz and TTz, are also very promising for achieving high performance, solution-processable small molecular OSCs. We believe this is the first report of the synthesis of thiazole-based D-A conjugated small molecules and the PCE of ~2.4% for **M2**:$PC_{71}BM$ device is the highest PCE so far for small molecule organic solar cell based on a small molecule (**M2**) with a band gap above 2.2 eV. Furthermore, we expect that the solar cell performances could be further improved through modification of the device morphology (using co-solvent, annealing, and processing additives). Additionally, designing a new molecular structure with thiazole derivatives as mentioned above may also provide better tuning for seeking a desirable band gap and energy levels, thereby enabling better performance. Continued work in this direction is being performed in our laboratory and will be presented in a subsequent report.

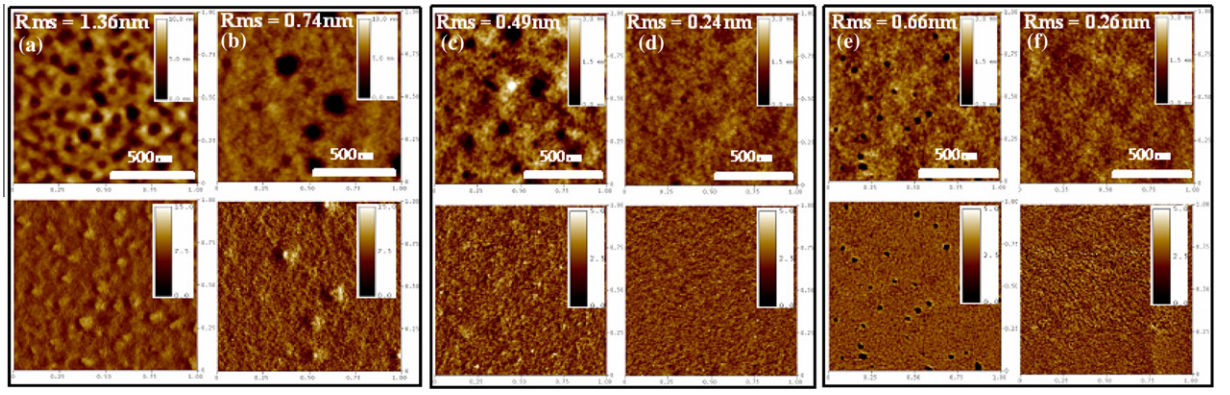

Fig. 4. AFM images (1 μm × 1 μm) (first row: height image; second row: phase image) of blend films spin-coated from chloroform: (a) **M1**/$PC_{61}BM$ (1:3 w/w), (b) **M2**/$PC_{61}BM$ (1:3 w/w), (c) **M1**/$PC_{71}BM$ (1:3 w/w), (d) **M2**/$PC_{71}BM$ (1:3 w/w); and from chlorobenzene: (e) **M1**/$PC_{71}BM$ (1:3 w/w), (f) **M2**/$PC_{71}BM$ (1:3 w/w).

Acknowledgements

This work was supported by the New & Renewable Energy program of the Korea Institute of Energy Technology Evaluation and Planning (KETEP) Grant (No. 20103020010050) funded by the Ministry of Knowledge Economy, Republic of Korea. This research was also supported by the Pioneer Research Center Program through the National Research Foundation of Korea funded by the Ministry of Education, Science and Technology (Contract No. 2008-05103).

Appendix A. Supplementary data

Supplementary data associated with this article can be found, in the online version, at doi:10.1016/j.orgel.2011.11.016.

References

[1] (a) J. Chen, Y. Cao, Acc. Chem. Res. 42 (2009) 1709;
(b) P.T. Boudreault, A. Najari, M. Leclerc, Chem. Mater. 23 (2011) 456.
[2] (a) H.-Y. Chen, J. Hou, S. Zhang, Y. Liang, G. Yang, Y. Yang, L. Yu, Y. Wu, G. Li, Nat. Photonics 3 (2009) 649;
(b) Y. Liang, Z. Xu, J. Xia, S.-T. Tsai, Y. Wu, G. Li, C. Ray, L. Yu, Adv. Mater. 22 (2010) E135;
(c) H. Zhou, L. Yang, A.C. Stuart, S.C. Price, S. Liu, W. You, Angew. Chem. Int. Edit. 50 (2011) 2995;
(d) S.C. Price, A.C. Stuart, L. Yang, H. Zhou, W. You, J. Am. Chem. Soc. 133 (2011) 4625;
(e) L. Huo, S. Zhang, X. Guo, F. Xu, Y. Li, J. Hou, Angew. Chem. Int. Edit. 50 (2011) 9697;
(f) Z. He, C. Zhong, X. Huang, W.-Y. Wong, H. Wu, L. Chen, S. Su, Y. Cao, Adv. Mater. 23 (2011) 4636.
[3] (a) M.T. Lloyd, A.C. Mayer, S. Subramanian, D.A. Mourey, D.J. Herman, A.V. Bapat, J.E. Anthony, G.G. Malliaras, J. Am. Chem. Soc. 129 (2007) 9144;
(b) N.M. Kronenberg, M. Deppisch, F. Würthner, H.W.A. Lademann, K. Deing, K. Meerholz, Chem. Commun. (2008) 6489.
[4] (a) C.Q. Ma, M. Fonrodona, M.C. Schikora, M.M. Wienk, R.A.J. Janssen, P. Bäuerle, Adv. Funct. Mater. 18 (2008) 3323;
(b) X. Sun, Y. Zhou, W. Wu, Y. Liu, W. Tian, G. Yu, W. Qiu, S. Chen, D. Zhu, J. Phys. Chem. B 110 (2006) 7702.
[5] (a) C. He, Q. He, X. Yang, G. Wu, C. Yang, F. Bai, Z. Shuai, L. Wang, Y. Li, J. Phys. Chem. C 111 (2007) 8661;
(b) C. He, Q. He, Y. Yi, G. Wu, F. Bai, Z. Shuai, Y. Li, J. Mater. Chem. 18 (2008) 4085;
(c) G. Zhao, G. Wu, C. He, F.-Q. Bai, H. Xi, H.-X. Zhang, Y. Li, J. Phys. Chem. C 113 (2009) 2636;
(d) J. Zhang, Y. Yang, C. He, Y. He, G. Zhao, Y. Li, Macromolecules 42 (2009) 7619.
[6] J. Zhang, D. Deng, C. He, Y. He, M. Zhang, Z.-G. Zhang, Z. Zhang, Y. Li, Chem. Mater. 23 (2011) 817.
[7] (a) L. Xue, J. He, X. Gu, Z. Yang, B. Xu, W. Tian, J. Phys. Chem. C 113 (2009) 12911;
(b) Z. Li, J. Pei, Y. Li, B. Xu, M. Deng, Z. Liu, H. Li, H. Lu, Q. Li, W. Tian, J. Phys. Chem. C 114 (2010) 18270;
(c) Z. Li, Q. Dong, Y. Li, B. Xu, M. Deng, J. Pei, J. Zhang, F. Chen, S. Wen, Y. Gao, W. Tian, J. Mater. Chem. 21 (2011) 2159.
[8] (a) A.B. Tamayo, B. Walker, J. Phys. Chem. C 112 (2008) 11545;
(b) A.B. Tamayo, X.-D. Dang, B. Walker, J.H. Seo, T. Kent, T.-Q. Nguyen, Appl. Phys. Lett. 94 (2009) 103301;
(c) J. Peet, A.B. Tamayo, X.-D. Dang, J.-H. Seo, T.-Q. Nguyen, Appl. Phys. Lett. 93 (2008) 163306;
(d) B. Walker, A.B. Tamayo, X.D. Dang, P. Zalar, J.H. Seo, A. Garcia, M. Tantiwiwat, T.-Q. Nguyen, Adv. Funct. Mater. 19 (2009) 3063.
[9] H. Burckstummer, N.M. Kronenberg, M. Gsanger, M. Stolte, K. Meerholz, F. Wurthner, J. Mater. Chem. 20 (2010) 240.
[10] (a) F. Silvestri, M.D. Irwin, L. Beverina, A. Facchetti, G.A. Pagani, T.J. Marks, J. Am. Chem. Soc. 130 (2008) 17640;
(b) D. Bagnis, L. Beverina, H. Huang, F. Silvestri, Y. Yao, H. Yan, G.A. Pagani, T.J. Marks, A. Facchetti, J. Am. Chem. Soc. 132 (2010) 4074;
(c) U. Mayerhoffer, K. Deing, K. Gruss, H. Braunschweig, K. Meerholz, F. Wurthner, Angew. Chem. Int. Edit. 48 (2009) 8776.
[11] (a) T. Rousseau, A. Cravino, T. Bura, G. Ulrich, R. Ziessel, J. Roncali, Chem. Commun. (2009) 1673;
(b) T. Rousseau, A. Cravino, T. Bura, G. Ulrich, R. Ziessel, J. Roncali, J. Mater. Chem. 19 (2009) 2298;
(c) T. Rousseau, A. Cravino, E. Ripaud, P. Leriche, S. Rihn, A. De Nicola, R. Ziessel, J. Roncali, Chem. Commun. 46 (2010) 5082.
[12] J. Mei, K.R. Graham, R. Stalder, J.R. Reynolds, Org. Lett. 12 (2010) 660.
[13] P. Dutta, W. Yang, S.H. Eom, W.H. Lee, I.N. Kang, S.-H. Lee, Chem. Commun. 48 (2012) 573.
[14] J. Zhou, X. Wan, Y. Liu, G. Long, F. Wang, Z. Li, Y. Zuo, C. Li, Y. Chen, Chem. Mater. 23 (2011) 4666.
[15] (a) S. Ando, J. Nishida, Y. Inoue, S. Tokito, Y. Yamashita, J. Mater. Chem. 14 (2004) 1787;
(b) I. Osaka, R. Zhang, G. Sauvé, D.M. Smilgies, T. Kowalewski, R.D. McCullough, J. Am. Chem. Soc. 131 (2009) 2521;
(c) I. Osaka, G. Sauvé, R. Zhang, T. Kowalewski, R.D. McCullough, Adv. Mater. 19 (2007) 4160.
[16] D.H. Kim, B.L. Lee, H. Moon, H.M. Kang, E.J. Jeong, J.-Il. Park, K.M. Han, S. Lee, B.W. Yoo, B.W. Koo, J.Y. Kim, W.H. Lee, K. Cho, H.A. Becerril, Z.N. Bao, J. Am. Chem. Soc. 131 (2009) 6124.
[17] (a) J. Lee, B.J. Jung, S.K. Lee, J.I. Lee, H.J. Cho, H.K. Shim, J. Polym. Sci., Part A: Polym. Chem. 43 (2005) 1845;
(b) M. Zhang, H. Fan, X. Guo, Y. He, Z. Zhang, J. Min, J. Zhang, G. Zhao, X. Zhan, Y. Li, Macromolecules 43 (2010) 5706.
[18] M. Yang, B. Peng, B. Liu, Y. Zou, K. Zhou, Y. He, C. Pan, Y. Li, J. Phys. Chem. C 114 (2010) 17989.
[19] I.H. Jung, J. Yu, E. Jeong, J. Kim, S. Kwon, H. Kong, K. Lee, H.Y. Woo, H.-K. Shim, Chem. Eur. J. 16 (2010) 3743.
[20] P. Dutta, W. Yang, H. Park, M. Baek, Y.S. Lee, S.H. Lee, Synth. Met. 161 (2011) 1582.
[21] M. Zhang, X. Guo, Y. Li, Adv. Energy Mater. 1 (2011) 557.
[22] (a) Y. Li, T.H. Kim, Q. Zhao, E.K. Kim, S.H. Han, Y.H. Kim, J. Jang, S.K. Kwon, J. Polym. Sci., Part A: Polym. Chem. 46 (2008) 5115;
(b) K. Suzuki, M. Tomura, S. Tanakaa, Y. Yamashita, Tetrahedron Lett. 41 (2000) 8359;
(c) M. He, T.M. Leslie, J.A. Sinicropi, S.M. Garner, L.D. Reed, Chem. Mater. 14 (2002) 4669.
[23] S.K. Lee, J.M. Cho, Y. Goo, W.S. Shin, J.C. Lee, W.H. Lee, I.N. Kang, H.K. Shim, S.J. Moon, Chem. Commun. 47 (2011) 1791.
[24] Q. Shi, H. Fan, Y. Liu, W. Hu, Y. Li, X. Zhan, J. Phys. Chem. C 114 (2010) 16843.
[25] L. Huo, X. Guo, S. Zhang, Y. Li, J. Hou, Macromolecules 44 (2011) 4035.
[26] Z-G. Zhang, J. Min, S. Zhang, J. Zhang, M. Zhang, Y. Li, Chem. Commun. 47 (2011) 9474.
[27] H. Shang, H. Fan, Q. Shi, S. Li, Y. Li, X. Zhan, Sol. Energy Mater. Sol. Cells 94 (2010) 457.
[28] (a) Z. Li, J. Ding, N. Song, J. Lu, Y. Tao, J. Am. Chem. Soc. 132 (2010) 13160;
(b) C. Duan, W. Cai, F. Huang, J. Zhang, M. Wang, T. Yang, C. Zhong, X. Gong, Y. Cao, Macromolecules 43 (2010) 5262.
[29] J.H. Hou, Z.A. Tan, Y. Yan, Y.J. He, C.H. Yang, Y.F. Li, J. Am. Chem. Soc. 128 (2006) 4911.
[30] (a) Y. He, Y.F. Li, Phys. Chem. Chem. Phys. 13 (2011) 1970;
(b) C.J. Brabec, C. Winder, N.S. Sariciftic, J.C. Hummelen, A. Dhanabalan, P.A. van Hal, R.A.J. Janssen, Adv. Funct. Mater. 12 (2002) 709.
[31] S.E. Shaheen, C.J. Brabec, N.S. Sariciftci, Appl. Phys. Lett. 78 (2001) 841.
[32] M.C. Scharber, D. Mühlbacher, M. Koppe, P. Denk, C. Waldauf, A.J. Heeger, C.J. Brabec, Adv. Mater. 18 (2006) 789.
[33] B.C. Thompson, J.M.J. Fréchet, Angew. Chem. Int. Edit. 47 (2008) 58.
[34] M.M. Wienk, J.M. Kroon, W.J.H. Verhees, J. Knol, J.C. Hummelen, P.A. van Hal, R.A.J. Janssen, Angew. Chem. Int. Edit. 42 (2003) 3371.
[35] A.P. Zoombelt, M. Fonrodona, M.G.R. Turbiez, M.M. Wienk, R.A.J. Janssen, J. Mater. Chem. 19 (2009) 5336.
[36] Y. Yang, J. Zhang, Y. Zhou, G. Zhao, C. He, Y. Li, M. Andersson, O. Ingans, F. Zhang, J. Phys. Chem. C 114 (2010) 3701.
[37] M.M. Mandoc, L.J.A. Koster, P.W.M. Blom, Appl. Phys. Lett. 90 (2007) 133504.
[38] X. Yang, J. Loos, Macromolecules 40 (2007) 1353.
[39] B. Walker, A. Tamayo, D.T. Duong, X-D. Dang, C. Kim, J. Granstrom, T.-Q. Nguyen, Adv. Energy Mater. 1 (2011) 221.
[40] H. Choi, S. Paek, J. Song, C. Kim, N. Cho, J. Ko, Chem. Commun. 47 (2011) 5509.
[41] Z. Li, Q. Dong, B. Xu, H. Li, S. Wen, J. Pei, S. Yao, H. Lu, P. Li, W. Tian, Sol. Energy Mater. Sol. Cells 95 (2011) 2272.